"Molecular layer deposition of a hafnium-based hybrid thin film as an electron beam resist," J. Shi, A. Ravi, N. E. Richey, H. Gong, and S. F. Bent, *ACS Applied Mat. & Inter.,* **14** (2022), 27140–27148, Accepted Version

Molecular Layer Deposition of a Hafnium-based Hybrid Thin Film as an Electron Beam Resist

Jingwei Shi[1], Ajay Ravi[1], Nathaniel E. Richey[1], Huaxin Gong[1], Stacey F. Bent[1,*]

[1]Department of Chemical Engineering, Stanford University, Stanford, California 94305, United States

*Corresponding Author: sbent@stanford.edu

Keywords: Atomic Layer Deposition, Molecular Layer Deposition, Lithography, Photoresist, E-beam Resist, Vapor-phase deposition

Abstract

The development of new resist materials is vital to fabrication techniques for next-generation microelectronics. Inorganic resists are promising candidates because they have higher etch resistance, are more impervious to pattern collapse, and are more absorbing of extreme ultraviolet (EUV) radiation than organic resists. However, there is limited understanding about how they behave under irradiation. In this work, a Hf-based hybrid thin film resist, known as "hafnicone", is deposited from the vapor-phase via molecular layer deposition (MLD) and its electron-beam and deep ultra-violet (DUV) induced patterning mechanism is explored. The hafnicone thin films are deposited at 100 °C using the Hf precursor tetrakis(dimethylamido)hafnium(IV) and the organic precursor ethylene glycol. E-beam lithography, scanning electron microscopy and profilometry are used to investigate the resist performance of hafnicone. Using 3M HCl as the developer, hafnicone behaves as a negative tone resist which exhibits a sensitivity of 400 $\mu C/cm^2$ and the ability to resolve 50 nm line widths. The resist is characterized via x-ray photoelectron spectroscopy (XPS) and infrared spectroscopy (IR) to investigate the patterning mechanism, which is described in the context of classical nucleation theory. This study of hafnicone hybrid MLD demonstrates the ability for the bottom-up vapor-deposition of inorganic resists to be utilized in advanced e-beam and DUV lithographic techniques.

Introduction

Continued development of lithographic techniques and material systems is critical for the fabrication of increasingly smaller microelectronic devices and the continued progression of Moore's law. The top-down fabrication approach remains the prevailing technique in the microelectronics industry,[1,2] which is a subtractive process in which nanostructures are carved out of bulk substrates. Lithography plays a central role in the top-down approach,[1] in which a desired pattern is created in a sacrificial layer, called the resist, which is deposited onto the substrate. Subsequent etch and deposition steps are carried out to generate 3D structures based on the pattern created on the resist. One type of resist, termed an inorganic resist,[2–7] is attracting increased attention. These resists consist of inorganic nanoparticles such as hafnium oxide,[8–11] titanium oxide,[11] or zirconium oxide[11,12] that are surface decorated with organic ligands such as methacrylic acid. These inorganic resists have several advantages over their organic counterparts: they are more resistant to etching, especially dry etching, are more absorbing of extreme ultraviolet (EUV), and are more resistant to pattern collapse because they are structurally more stable.[2] Resists can be sensitive to light or electrons, acting as either a photoresist or e-beam resist, respectively. Deep ultra-violet (DUV) and EUV photolithography are the most prevalent techniques used in industry; however, electron beam lithography is also important and remains the dominant technique in research settings as well as small scale industrial processes because of its mask-less nature (direct-write) and ease in achieving very high resolution (sub-10 nm).[1]

As industry trends towards smaller feature sizes, there is a growing need for alternative methods to deposit lithographic resists with a high degree of control at nanoscale thickness.[1] Moreover, vapor deposition of the e-beam or photo-resist, instead of the more common spin coating,[1] would provide several advantages: (1) vacuum vapor deposition may be more amenable to the typical process conditions for nanofabrication and lithography, which occur in vacuum; (2) the need to bake the resist to remove the carrier solvent can be eliminated, which means a theoretically lower processing temperature; (3) conformal resist coatings better allow for the fabrication of structures on topologically complex, 3D substrates compared to spin-coat resist methods, for which complicated modifications are required to coat non-planar surfaces.[13] One deposition method that possesses many of these capabilities is atomic or molecular layer deposition (ALD or MLD). The semiconductor industry already employs ALD in part of their process flow. ALD (and MLD) are used in industry because they can deposit surface coatings with accurate composition and thickness. Although this layer-by-layer deposition technique is primarily used to deposit dielectrics, such as HfO_2[9] and Al_2O_3,[10] in applications such as logic gates or dynamic random access memory (DRAM), there is opportunity to expand the technique to resist deposition. Reports of vapor deposited, bottom-up deposition of resists are limited,[14–17] and the specific utilization of ALD or MLD has only been applied for organic resists.[15,18] Coincidentally, the coordination polymers that can be readily deposited via MLD[19] are very similar compositionally to the inorganic resists reported above. Due to the layer-by-layer nature of MLD, there is control over the composition of the grown material, and even ternary (multiple metal or ligands) materials can be synthesized.[20] Also, due to the self-limiting nature of MLD, it holds advantages as a vapor deposition method for the conformal coating of

resist material on non-planar surfaces. Hence, it is worthwhile to study the resist properties of these MLD-grown coordination polymers as a potential approach to develop inorganic resists for next-generation microelectronics processing.

In this work, we demonstrate the feasibility of MLD for the vapor-phase deposition of thin film inorganic resists. We investigate the use of an MLD hafnium-based hybrid thin film as both an e-beam and DUV resist. The resist film is synthesized using tetrakis(dimethylamino)hafnium(IV) (TDMAHf) and ethylene glycol (EG) as the hafnium and organic precursor, respectively. Hafnium-based hybrids, termed "hafnicones", hold special interest because hafnium has a high absorbance cross-section in the DUV and extreme ultraviolet (EUV) for a metal.[21] We examine the hafnicone resist performance and pattern-ability via contrast and development curves and demonstrate the ability to resolve 50 nm line widths. Furthermore, we study the patterning mechanism and show that the same mechanism operates under both e-beam and DUV irradiation. As a proxy for EUV irradiation studies, which are difficult due to the scarcity of EUV lithography setups, we employ e-beam lithography to mimic the generation of secondary electrons that are hypothesized to be ultimately responsible for the solubility switch reactions in EUV processes.[22] While hafnium-based inorganic resists[8–11] and vapor deposited resists[14–17] have been studied before, this study lays the groundwork for the use of vapor-phase MLD in the deposition of hybrid inorganic-organic thin films for e-beam or photo-resist applications. Along with conformality of high aspect ratio non-planar substrates, MLD allows for fine compositional control: with many metal and organic precursors to choose from, this deposition technique allows for a wide design and parameter space to create and

tune inorganic resists with better lithographic performance to advance device fabrication processes.

Experimental

Chemicals: Tetrakis(dimethylamino)hafnium(IV) (TDMAHf) was purchased from Strem Chemicals and anhydrous ethylene glycol (EG) was purchased from Sigma Aldrich. All chemicals were stored in the glove box for storage and used as received. Thin films were deposited on n-doped (100) Si substrates with 1.5 nm native oxide from WRS Materials. Prior to deposition, substrates were first sonicated in deionized water for 10 minutes, dried with air, and then cleaned for 15 minutes in a Novascan PSD Series Digital UV Ozone System to remove any remaining organic contamination.

Deposition: Depositions were carried out in a home-built warm-walled tube reactor as described previously, with modifications to the hafnicone deposition process conditions described below.[23–25] The reactor was pumped by a Leybold Trivac rotary vane pump and continuously purged with 10 SCCM of dry N_2. Depositions were carried out at a reactor stage temperature of 100 °C for a total of 200 MLD cycles. The transfer lines and bubblers containing TDMAHf and EG were heated to 45 °C and 55 °C, respectively. A hafnicone MLD cycle consisted of two temporally separated half cycles, in which TDMAHf followed by EG was introduced into the reactor. Each precursor half cycle was comprised of three steps: (1) dose, in which the precursor was introduced into the chamber; (2) soak, in which the nitrogen and the pump lines were closed so that the dosed precursor vapor could remain in the reactor to react; (3) purge,

in which both nitrogen and pump lines were opened to the chamber to remove all unreacted precursors and byproducts. The dose, soak, and purge times for both precursors were 1 s, 20 s, and 60 s, respectively.

Electron-beam lithography and development: Electron-beam lithography (EBL) was performed on a Raith VOYAGER electron beam lithography system, operated at 50 keV and 5 nA. Lithographic patterns were designed in KLayout. The compatibility of various developers were tested with the hafnicone resist, shown in SI Figure S6, and 3M HCl was chosen as the negative developer, and substrates were typically developed for 3 minutes and then rinsed with DI water. Typical base doses for the dose matrix pattern were 50 $\mu C/cm^2$ and 100 $\mu C/cm^2$. For the dose matrix pattern, the dose factor multiplied by a preset base dose determines the final exposure level per area. For measurements that required a blanket instead of a patterned sample, such as for IR or XPS, a much larger area of 1 cm^2 was exposed in the e-beam lithography system, as shown in Figure S5a.

DUV exposure and development: A 254 nm handheld DUV light lamp (Cole-Parmer, intensity of 280 $\mu W/cm^2$ as measured by a Newport 91150V Reference Cell and Meter) was used to test the DUV sensitivity of hafnicone. Flood exposure tests were performed for 30 minutes which corresponds to doses of 500 mJ/cm^2. Development conditions were the same as for e-beam exposed samples.

Characterization: The thicknesses of the deposited films were determined by variable angle spectroscopic ellipsometry (VASE) using a J. A. Woollam Co. α-SE spectroscopic ellipsometer with a spectral range of 300-900 nm. X-ray photoelectron spectroscopy (XPS) was

performed on a PHI 5000 Versaprobe 3 with a monochromatic Al Kα X-ray source at 1486 eV. Prior to XPS analysis, samples were sputter cleaned of adventitious carbonaceous species via gas cluster ion beam (GCIB) sputtering. Survey scans were performed with 3 passes at 224 eV pass energy while high resolution scans were done with 5 passes at 55 eV pass energy.

Attenuated total reflection Fourier transform infrared spectroscopy (ATR-FTIR) was performed using a Nicolet iS50 FTIR spectrometer with a Harrick VariGATR attachment and a HgCdTe detector. FTIR spectra were taken with 64 scans at 2 cm^{-1} resolution. Surface morphology and pattern development were probed with profilometry using a Bruker Pektak XT-A, where typical line scans were 1200 μm and used 1mg force probe, and scanning electron microscopy using a FEI Magellan 400 XHR SEM, operated at 1keV to improve surface sensitivity and contrast.

Results and Discussion

MLD of hafnicone: The growth characteristics of hafnicone were reported in an earlier paper by our group.[25] For this study, we performed 200 hafnicone MLD cycles, which resulted in a film thickness of 300 ± 8 Å (error bar is one standard deviation) as measured by VASE. The resulting GPC of 1.5 Å/cycle is slightly higher than our previous reported saturating growth rate of 1.4 Å/cycle.[25] This small difference in growth rates is within the uncertainty of the measurement, but may also be related to the lower deposition temperature of the present work compared to the earlier study, which was performed at 110 °C instead of 100 °C, since there is a slight temperature dependence of GPC even within the MLD window.[26] The lower

deposition temperature may also lead to elevated GPC if a slight chemical vapor deposition (CVD) growth component is present due to insufficient purging.

The elemental composition and oxidation state of the deposited hafnicone film were probed via XPS, with the spectra shown in Figure 1. The survey scan shown in Figure 1a reveals that the as-deposited hafnicone film contains only the expected elements of Hf, O, and C. The Hf 4f high-resolution scan shown in Figure 1b reveals that the Hf is present as Hf(IV), which is expected since the TDMAHf precursor is in the +4 oxidation state and the reaction between the two precursors is likely a ligand exchange reaction with no change in oxidation state.

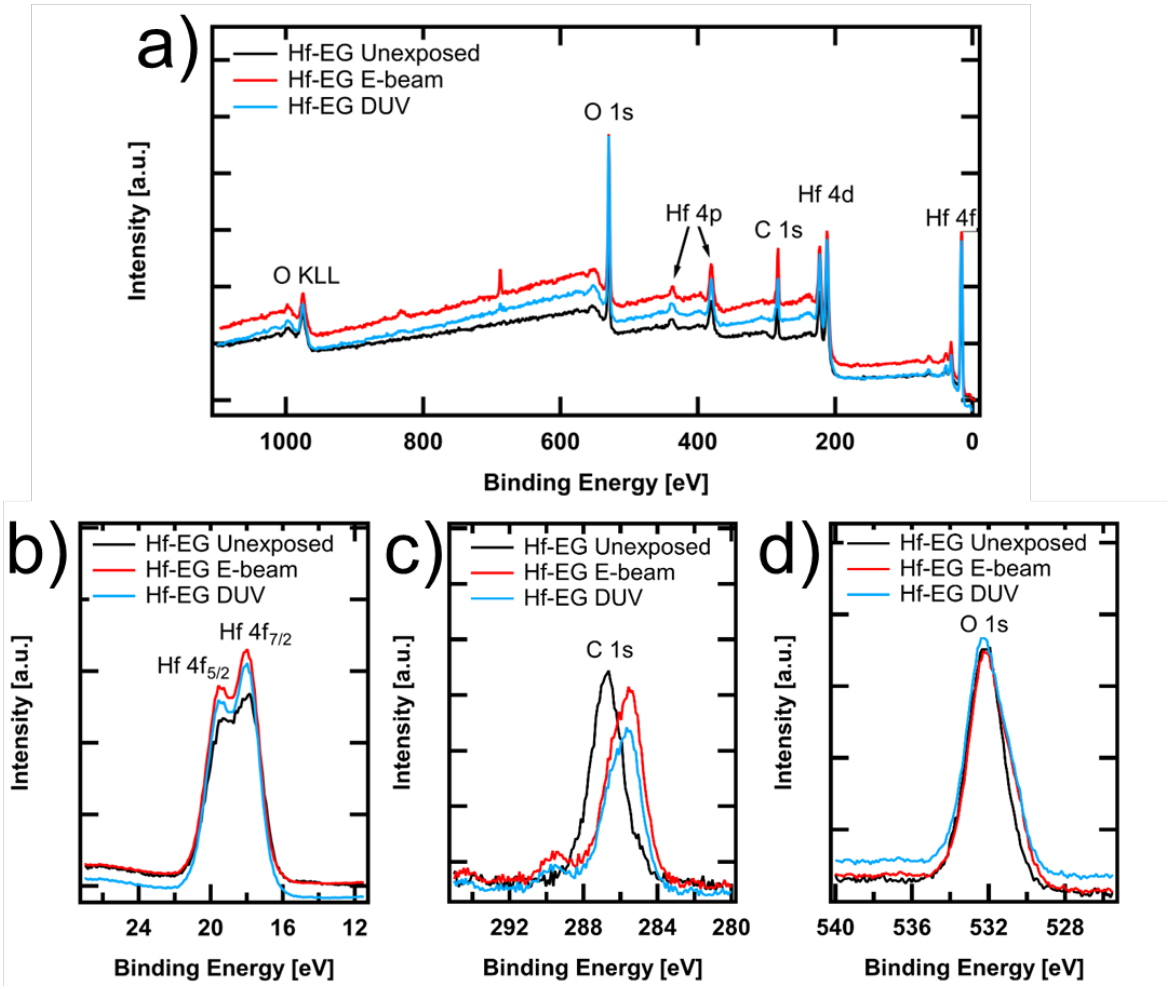

Figure 1 (a) XPS survey scan of hafnicone films. (b) XPS Hf 4f high-resolution scan. (c) XPS C 1s high-resolution scan. (d) XPS O 1s high-resolution scan. All spectra shown for hafnicone film as-deposited and after e-beam or DUV exposure and development in 3 M HCl for 3 min. The peak near 700 eV in the XPS survey arises from fluorine contamination at an elemental composition of less than 1%.

The C 1s high-resolution scan plotted in Figure 1c shows that the carbon in the unexposed, as-deposited hafnicone film matches that of carbon bonded to oxygen, which appears at 286.7 eV.[27] The O1s high-resolution scan shown in Figure 1d, which has a peak

located at 532.1 eV, is also consistent with the oxygen being bound to carbon and hafnium.[28] For reference, oxygen in the unreacted EG precursor appears at 533.0 eV;[29] however, it is reasonable that the ligand exchange reaction and the subsequent bonding change from C-O-H to C-O-Hf can cause a downshift of this binding energy value. The experimental elemental ratio of Hf:C:O determined from the XPS survey scan is 1:4.4:4.4, which is close to the expected nominal ratio of 1:4:4 for a hafnicone film with an ideal stoichiometry of $Hf(C_2H_4O_2)_4$. However, the quantification of the elemental ratios of hafnicone should be treated with caution due to the presence of adventitious carbon.

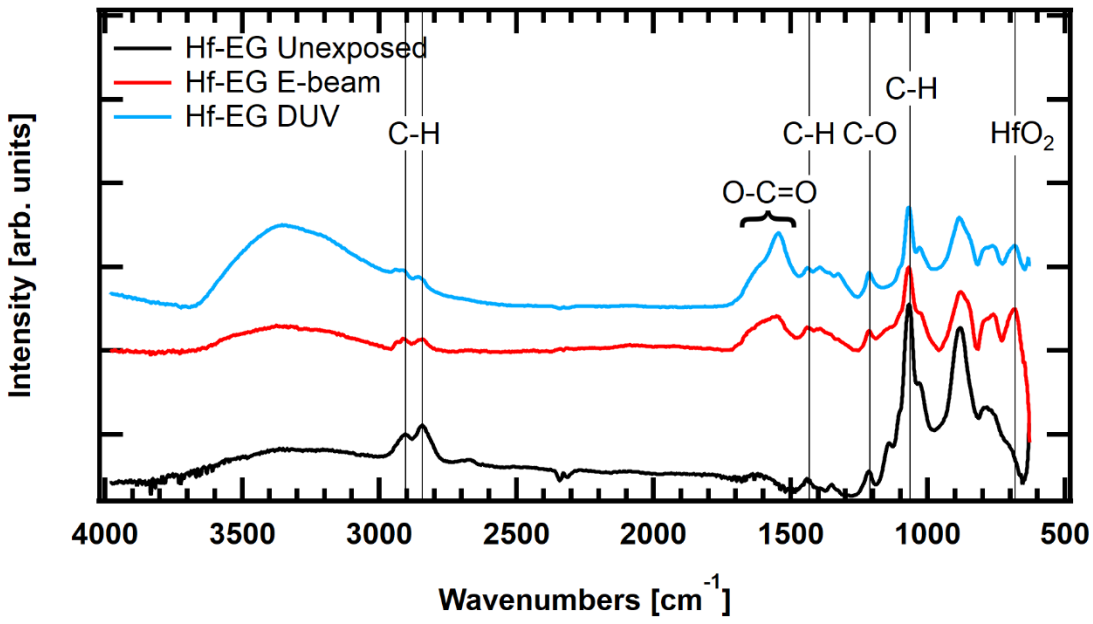

Figure 2: IR spectra of hafnicone film as-deposited and after e-beam or DUV exposure and development in 3 M HCl for 3 min, with key vibrational modes indicated. The spectrum in red was collected for a hafnicone film with e-beam exposure of 500 μC/cm^2, and the spectrum in blue was collected for a hafnicone film exposed to 30 min of a 254 nm DUV light source.

IR spectroscopy was performed on the as-deposited (unexposed) hafnicone films to confirm the chemical bonding. In the resulting spectra, shown in Figure 2, there are peaks associated with both C-H (2844, 2909, 1441, 1070 cm^{-1}) and C-O (1214 cm^{-1}) vibrational modes, which is expected for the MLD material since EG linkers are present. There is a notable absence of a mode corresponding to amorphous HfO_2, located at 680 cm^{-1},[30,31] which suggests the as-deposited thin films have not degraded or formed hafnium oxide as a contaminant.

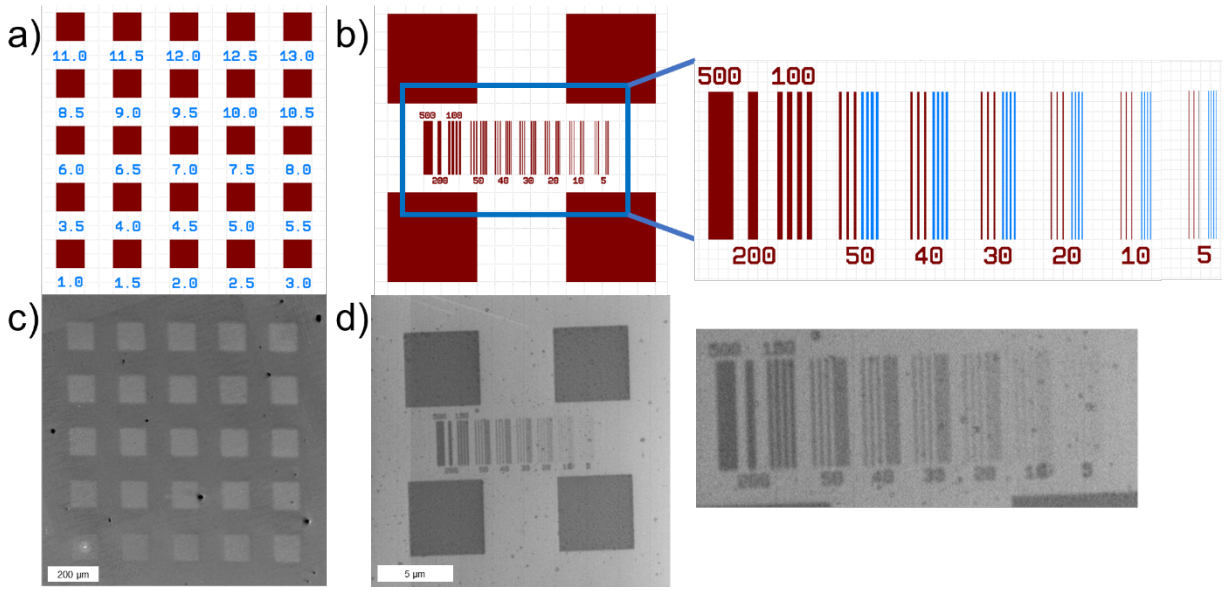

Figure 3: (a) Dose matrix pattern, with numbers under each box representing the dose factor. The dose factor multiplied by a preset base dose determines the final exposure level per area. (b) Simple box and grating pattern used in the study, with numbers under grating representing the width of the lines in nm. Lines were spaced 100 nm (red lines in inset) and 50 nm (blue lines

in inset) apart. (c) SEM image of a representative 30 nm hafnicone sample exposed to the dose matrix pattern with base dose of 100 μC/cm^2 after development in 3M HCl for 3 min. (d) SEM image of a representative sample exposed to the box and grating pattern after development in 3M HCl for 3 min. Exposed resist condition was 500 μC/cm^2 for the box and grating pattern.

Electron-beam lithography (EBL) on hafnicone films: The deposited hafnicone films were tested for resist behavior by exposure to an electron beam. The EBL pattern files are shown in Figure 3a,b. The dose matrix pattern represented in Figure 3a was used to investigate the sensitivity of the hafnicone resist; the resulting SEM image of the developed pattern is shown in Figure 3c. Profilometry measurements of the dose matrix pattern using a base dose of 50 μC/cm^2 were used to generate the resist contrast curve shown in Figure 4a; the raw height scans are shown in SI Figure S1. The sensitivity of the hafnicone film, defined as the critical electron dose at which normalized thickness equals 1 in the resist contrast curve, is determined to be 400 μC/cm^2. In addition, the contrast, which represents the ability of the resist to differentiate between exposed and unexposed areas, is calculated based on the data in Figure 4a using the equation $\gamma = 1/\log_{10}(D_{100}/D_0)$ to be 1.1; here D_{100} represents the sensitivity and D_0 represents the maximum dose for which the resist remains completely undeveloped.

Next a simple box and grid pattern, shown in Figure 3b, was used to test the finest line pattern we could achieve with this MLD resist. In the box and grid pattern, the one-dimensional lines vary in line width from 100 nm to 5 nm and have two different line spacing of 100 nm and 50 nm. From the SEM image in Figure 3d, it can be seen that lines are well resolved at a line

width of 50 nm and line pitch of 100 nm. Lines become increasingly faint with reduction in line width: by 20 nm line widths, the contrast in SEM is quite poor. Additionally, when the line pitch is decreased from 100 nm to 50 nm, the lines become grouped together and are no longer well resolved. We note that the resolution limit of the EBL instrument is ~10 nm. The blurring and faintness of the line patterns below 50 nm is limited by the contrast of the resist.[32]

The developer and development time used in the experiments shown in Figures 3 and 4 were 3M HCl and 3 minutes, respectively. The developer was selected based on comparative studies with other acids and organic solvents. Besides 3 M HCl, blanket unexposed hafnicone films were tested in 1M HCl, acetic acid, DMSO, acetonitrile, and acetone to select the best negative developer, as shown in Figure S6. Only the 3 M HCl developer led to significant dissolution of the resist film by 10 minutes of development, and thus was chosen for the remainder of the studies. To determine the optimal development time, blanket hafnicone films were exposed using e-beam lithography and DUV; these exposed samples plus as-deposited, unexposed hafnicone films were immersed in 3M HCl developer and the resulting thicknesses were tracked via VASE (Figure 4b). We observe that after 3 minutes of development, the normalized thickness for the as-deposited hafnicone resist drops to <0.05, whereas the exposed resist remains approximately 1. Thus, this hafnicone thin film exhibits negative resist behavior using the 3M HCl developer and 3 minutes is sufficient for the desired contrast.

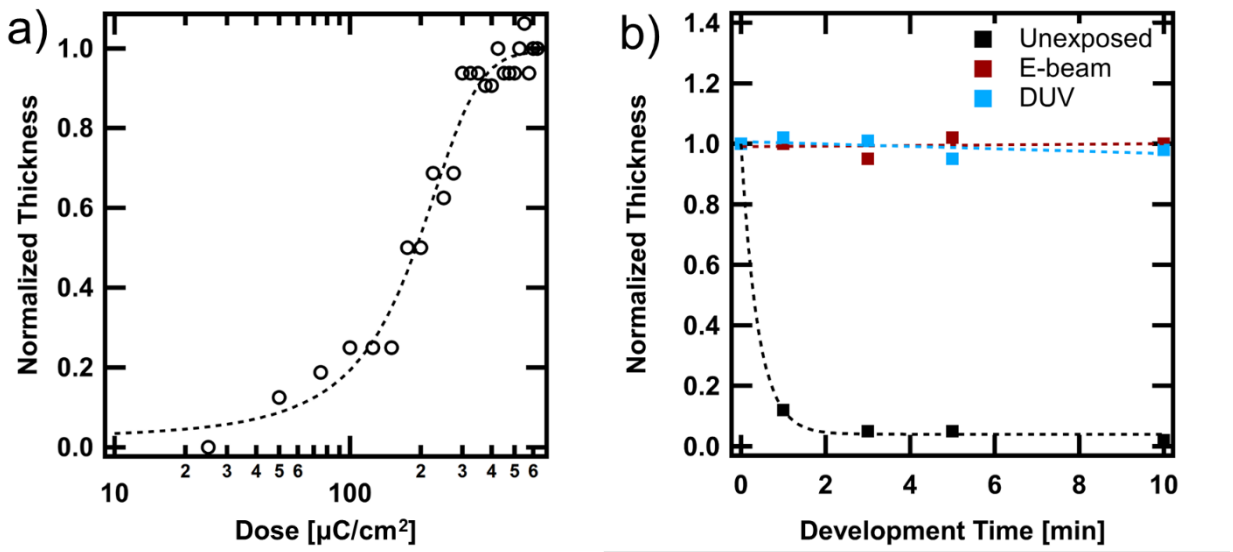

Figure 4: (a) Contrast curve of Hf-EG resist, developed with 3M HCl for 3 minutes. Normalized thickness is determined using profilometry on the dose matrix pattern (b) Development curves of Hf-EG resist, with 3M HCl as the negative developer. E-beam exposure was 500 μC/cm^2. DUV exposure was 500 mJ/cm^2. In (a), and (b), as-deposited hafnicone thickness was 30 nm for these studies.

To investigate the electron response mechanism, the resist was probed with XPS and IR spectroscopy after exposure and development to detect chemical changes in the film. The XPS survey scans in Figure 1a of the post-exposure and post-development resist reveal that the same elements are present as in the as-deposited hafnicone film. However, the high-resolution spectra of the O 1s and C 1s regions reveal significant changes. In the O 1s spectrum of the exposed resist, shown in Figure 1d, a shoulder feature emerges at lower binding energy. When fitted, as shown in SI Figure S2a, this shoulder corresponds to a peak at 530.0 eV, assigned to hafnium oxide.[33] The O 1s fit parameters, summarized in SI Table S1, indicate that oxygen as

hafnium oxide is 15% of the total oxygen present in the post-exposure resist. This result contrasts with the as-deposited O 1s spectra, shown in SI Figure S2b, in which negligible oxygen is present as hafnium oxide. The C 1s spectrum in Figure 1c also reveals changes upon electron irradiation: the post-exposed hafnicone shows two peaks, one at 289.5 eV[34] and one at 285.0 eV,[34] which correspond to carbon in carboxylate groups (O-C=O) and bonded to other carbon (C-C), respectively. Notably, the peak at 286.7 eV, which is associated with carbon present as C-O, is absent in the post-exposed spectrum. We hypothesize that the C-O bond is cleaved upon e-beam irradiation, and that the carbon radicals that form can subsequently react with ambient oxygen ex-situ or oxygen from the ethylene glycol ligand to form carboxylate species, which are observed in both XPS and IR (see below); the former reaction mechanism of carbon radicals with ambient oxygen post e-beam exposure is consistent with that attributed in the literature to the formation of carboxylates in PMMA resists.[35] Furthermore, the elemental ratio of Hf:C:O in the post-exposed hafnicone is 1:2.6:4.0, showing a significant decrease in the carbon content compared to the as-deposited hafnicone film. This result suggests that a portion of the carbon content leaves the film once the C-O bond is cleaved, consistent with the loss in carbon content observed in other inorganic resist systems after exposure.[2]

IR spectroscopy on the post-exposed and post-developed resist reveals the emergence of several peaks between 1300-1600 cm^{-1}, which can be attributed to C-O and C=O peaks found in carboxylate and carbonate moieties.[36,37] The presence of these species is consistent with the C 1s XPS spectra, which also show these oxidized carbon species. A peak also appears at ~680 cm^{-1}, which can be assigned to phonon modes of amorphous HfO_2.[30,31] The observation of the HfO_2 peak agrees with the O 1s XPS spectrum, which shows the appearance of HfO_2 species in

the exposed hafnicone resist film. Together with the XPS results, the IR spectrum indicates that the e-beam causes the hafnicone film to degrade and convert to HfO_2 and hafnium carboxylate and carbonate species.

We also performed a box and grid pattern experiment with a high electron beam dose to investigate any structural changes in the resist post-exposure. Three separate electron exposure doses were performed, 500, 1000, and a significantly higher exposure of 5000 $\mu C/cm^2$ to exaggerate any changes that the electron exposure may have on the resist. The developed EBL pattern was imaged with SEM, with the results shown in SI Figure S3a-c. There is evidence in the SEM image of significant HfO_2 nanoparticle formation, between 10 and 100nm in size, for the 1000 and 5000 $\mu C/cm^2$ exposure condition and minor nanoparticle formation at 500 $\mu C/cm^2$. This result contrasts with the unexposed hafnicone resist, shown in SI Figure S3d, which lacks any evident nanoparticles.

Response of Hafnicone Films to DUV Flood Exposure: In the DUV experiments, a shadow mask was used as a proof-of-concept to demonstrate the DUV patternability of the hafnicone resist. The pattern of the shadow mask is somewhat preserved (SI Figure S4), although we do observe blurring of the grating lines, attributed to the use of a rudimentary shadow mask instead of a photoresist mask with beam optics in a real photolithography system. Next, as with the EBL experiment, we investigated the development curve with 3M HCl, as shown in Figure 4b. The film shows very similar development characteristics and the same negative resist behavior as observed when e-beam exposed, and is also stable in the developer for at least 10 minutes. The

results show that the development of the DUV-exposed hafnicone is very similar compared to the electron-exposed hafnicone.

The DUV-exposed hafnicone film was also probed with XPS and IR spectroscopy to detect chemical changes in the film. XPS survey scans of the post-DUV exposure resist reveal a similar elemental composition to the as-deposited hafnicone resist, as shown in Figure 1a. The high-resolution scans of the O 1s and C 1s spectra reveal the same significant changes as the post e-beam exposure resist. The same shoulder feature in the O 1s scan is present in the DUV exposed resist as in the e-beam sample (Figure 1d). When fitted, as shown in SI Figure S1c, this shoulder peak appears at 530.0 eV, which corresponds to hafnium oxide.[33] The O 1s fit parameters, summarized in SI Table S2, indicate that oxygen in the form of hafnium oxide constitutes 20% of the total oxygen present in the post-exposure resist, similar to the hafnium oxide concentration in the post-e-beam resist (15%). Like the e-beam sample, the post DUV-exposed hafnicone film shows two peaks in the C 1s spectrum in Figure 1c, one at 289.5 eV[28] and one at 285.0 eV,[28] corresponding to carbon as O-C=O and C-C respectively. As was observed in the e-beam studies, this spectrum lacks a C-O peak, suggesting that DUV light also causes the C-O bond to cleave. With its Hf:C:O ratio equal to 1:2.7:4.0, the DUV exposed hafnicone film also contains substantially less carbon than it did before exposure.

IR spectroscopy performed on the hafnicone film after DUV exposure and development reveals similar behavior to the film after e-beam exposure and development. Several peaks emerge between 1300-1600 cm^{-1}, which can be attributed to C-O and C=O stretching vibrational modes found in carboxylate and carbonate moieties.[36,38] The same HfO_2 peak as seen in the e-beam exposed resist also emerges at ~680 cm^{-1}.[30,31] Together with the XPS results, the IR spectrum shows that similar chemical and structural changes occur in the DUV-exposed resist as in the e-beam exposed resist.

Figure 5 – Mechanism scheme

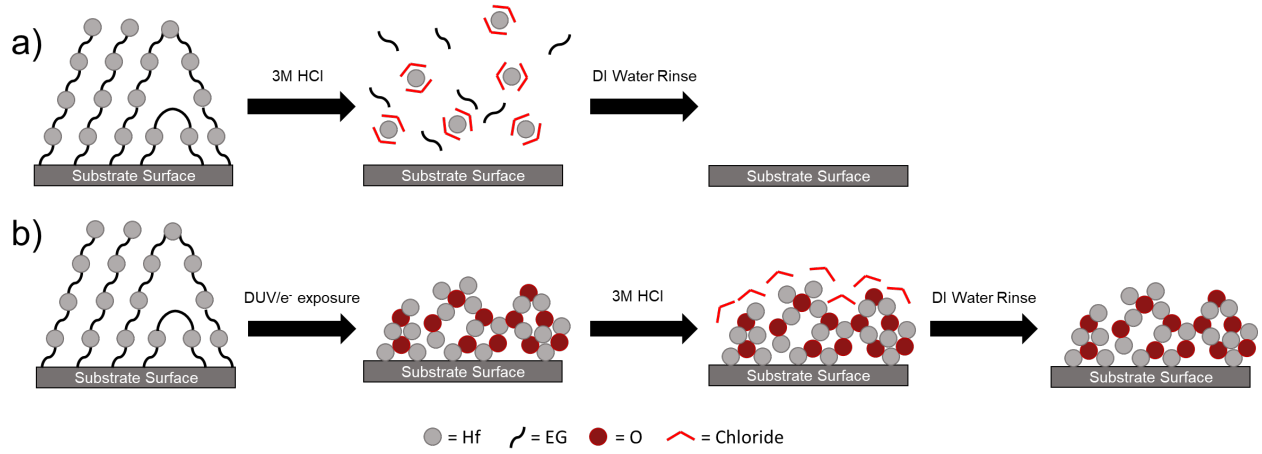

Figure 5: Patterning mechanism for hafnicone resist under DUV and e-beam exposure. (a) Without exposure, the hafnicone resist is dissolved in HCl via chloride ion chelation to hafnium ion centers. After DI rinse, the entire film is removed. (b) Post exposure, the C-O bond in the ethylene glycol unit is cleaved, allowing the hafnium oxide centers to aggregate and form HfO_x, which is more resistant to dissolution. After DI rinse, the hafnium oxide remains.

Patterning Mechanism: From the above data, we propose a chemical mechanism for the negative resist response of hafnicone in the HCl developer. The mechanism is illustrated schematically in Figure 5. Since the chemical changes for the DUV and e-beam exposed sample are very similar, we hypothesize that the underlying patterning mechanism is the same. This self-similarity in the patterning mechanism between the e-beam and light induced processes is also observed in other resist systems like poly(methyl methacrylate) (PMMA) or poly(methyl methacrylate-co-methacrylic acid) (AR-P 610).[39] Here, we posit that in the as-deposited films, the metal ion centers are solely coordinated to the oxygen in the ethylene glycol linkers as shown via the Hf 4f and O 1s high-resolution XPS spectra, which would be atomically sized Hf-O centers akin to a coordination polymer. Upon development of an unexposed film, the acid reacts with the Hf-O bond, likely protonating the alkoxide and forming a water-soluble $HfCl_x$ species (Figure 5a). This reaction explains the as-deposited hafnicone development curve in 3M HCl, with the normalized thickness dropping to <0.05 after 3 minutes of development.

Upon e-beam or DUV exposure, on the other hand, the data show that the C-O bond is cleaved and hafnium oxide and carboxylate species are formed; while the DUV exposure was done in ambient and the e-beam lithography performed under vacuum, we still see the same carboxylate and hafnium oxide species upon either form of irradiation. With DUV exposure, once the C-O bond is cleaved under DUV, carboxylates and hafnium oxide are formed upon reaction with ambient oxygen. With e-beam, while the exposure is done in vacuum, the carbon radicals that form can either react with the oxygen in ethylene glycol or with ambient oxygen post-exposure to form the carboxylate. Again, we see this latter mechanism is operative in the

formation of carbonyl and carboxylate species in the e-beam irradiation of PMMA and subsequent ex-situ study by XPS.[35]

We hypothesize that the exposure and subsequent bond cleavage and oxidation reactions cause the formation of inorganic hafnium oxide nanoparticles by allowing the hafnium oxide centers to aggregate (Figure 5b). These aggregated particles of HfO_x are more resistant to dissolution, since bulk hafnium oxide is not soluble in HCl, consistent with the experimental development curves for the post-exposure and post-development resist which show insolubility as well as the SEM images of nanoparticle formation of the developed resist in SI Figure S3a-c. This hypothesized mechanism also explains the limitations of the hafnicone resist in terms of patterning resolution. Because the irradiation causes the organic linkers to dissociate and lead to HfO_2 aggregation, the resolution will be limited by this particle formation and migration. In SEM images shown in Figure 3 and SI Figure S3, we see that the nanoparticles formed can exceed the smallest feature sizes.

We can further understand the e-beam and DUV response mechanism and the HfO_x nanoparticle formation from an energy-minimization argument in the context of classical nucleation theory.[40–42] Once the electron-beam or DUV light cleaves the C-O bond in ethylene glycol moieties in the hafnicone film, the initially atomically sized Hf-O centers in the as-deposited hafnium coordination polymer can reorganize and form HfO_x domains in the resist. For reference, in the literature on colloidal nanoparticle synthesis, for hafnium oxide and other oxides in general,[41–44] it is common that capping ligands are required on the surface of the nanoparticles to prevent their further growth and coalescence. Otherwise, past a critical radius, as dictated by classical nucleation theory, the nanoparticles will grow in size due to the

dominance of the volumetric Gibbs free energy term.[40] In an analogous fashion, the electron beam or DUV irradiation can provide the necessary thermal energy and cleavage of bonds to allow the unprotected HfO_x domains to become mobile and diffuse within the resist,[45] which allows a similar nucleation process to occur: as in colloidal nanoparticle synthesis, this nucleation process would be driven by the energy balance of surface energy and bulk Gibbs free energy of the Hf-O centers in the as-deposited hafnicone film once the organic ligand is cleaved. Once the HfO_x domains reach a certain size, the continued growth of the oxide domains becomes energetically favorable and the domains become larger. This nanoparticle aggregation behavior has already been shown to occur in metal oxide nanoparticle photoresists. In those systems, DUV irradiation is hypothesized to drive the unbinding of the organic ligands from the inorganic metal nanoparticles, which propels the sintering and agglomeration of the nanoparticles.[2,45] This increase in nanoparticle size causes the solubility change of these resist systems.[45] In our system, we posit that the cleaving of the C-O bond in the ethylene glycol ligand mimics this ligand unbinding and enables the process of HfO_x coalescence, inducing a similar solubility change.

With this description of the patterning mechanism, we can rationalize the similarity between the post DUV and post e-beam hafnicone resist. The result of both types of irradiation appears to be the cleavage of the C-O bond in the ethylene glycol linker, but how each exposure achieves this bond cleavage is different. Under irradiation by high energy (50 keV) electrons, the C-O bond in the hafnicone resist can directly cleave, as it does in pure ethylene glycol.[46] Unlike direct electron exposure, DUV exposure does not provide enough energy (254 nm corresponds to 4.8 eV) to directly ionize photoelectrons and can only create bound excited

states.[47] However, these excited electronic states decay thermally or photochemically[48–50] to cleave the C-O bond, resulting in the same end state. As a result, both types of exposure are sufficient for causing a solubility switch in the MLD hafnicone resist.

We also speculate that the hafnicone resists have potential for use as EUV resists. As a substitute for EUV irradiation studies, which is difficult due to the scarcity of EUV lithography setups, e-beam lithography may be used to mimic the generation of secondary electrons that are hypothesized to be ultimately responsible for the solubility switch reactions in EUV processes.[22] Furthermore, the presence of hafnium in the hafnicone film is appealing since among metals, hafnium has a high absorbance cross-section in the DUV and EUV.[21]

To summarize the proposed mechanism, the e-beam or DUV exposure induces a solubility switch in the hafnicone resist by cleaving the C-O bond in the ethylene glycol moieties in the resist, as seen via XPS and IR spectroscopy. This bond cleavage allows the initially atomically small HfO_x centers in the coordination polymer to reorganize and aggregate into HfO_x nanoparticle domains which are insoluble in HCl. The chemical and physical change of the resist then leads to the solubility change in the 3M HCl developer. The formation of visible nanoparticles upon exposure and development of hafnicone is an area of optimization for hybrid MLD resists. By selecting more strongly chelating organic ligands such as carboxylate, or choosing a metal for which the formation of oxide nanoparticles is less favorable such as zinc oxide compared to hafnium oxide, the resulting hybrid resist may be less likely to aggregate to as great an extent and hence avoid formation of large nanoparticles upon irradiation. This tuning of the resist components could potentially improve its resolution due to the mechanism described above.

Conclusions: We have shown that a hafnium-based hybrid thin film deposited via MLD can act as an e-beam resist. The as-deposited hafnicone thin film is characterized via XPS and IR spectroscopy and shows the expected bonding motifs and elemental composition ratio. When exposed to e-beam and DUV, the hafnicone thin film acts as a negative resist in 3M HCl developer. The resist demonstrates a sensitivity of 400 $\mu C/cm^2$ and the ability to be patterned to at least 50 nm line widths. The e-beam and DUV patterning mechanism is investigated via XPS and IR spectroscopy, showing that upon irradiation, the C-O bond in ethylene glycol cleaves. We propose that this bond cleavage allows the Hf-O domains to agglomerate and form hafnium oxide, driven by the energy minimization of surface energy and bulk Gibbs free energy in the context of nucleation theory, and that this resulting material is insoluble to the acid developer leading to the negative resist behavior observed. With this study, we demonstrate the first vapor-deposited, hybrid inorganic-organic resist. The ability to conformally coat existing structures with resist films via MLD may allow the development of new lithographic schemes to create novel architectures in multistep processes not possible with the use of spin-cast resists such as patterning steps on non-planar substrates. Furthermore, the inorganic nature of these hybrid resists means they may possess inherent advantages such as higher etch resistance, better resistance to pattern collapse, and potentially higher EUV absorbance, for emerging EUV techniques, compared to organic resists. With a wide range of metal and organic precursors to choose from, hybrid MLD allows for a broad design and parameter space to create optimized inorganic thin film resists for the continued development of more advanced lithographic processes.

Supporting Information: The SI includes profilometry data, XPS high-resolution scans, XPS peak deconvolution fitted parameters, SEM images, and development curve data.

Acknowledgements: This work was supported by the National Science Foundation (Grant CHE-1904108). J.S. acknowledges support from an NSF Graduate Research Fellowship (Grant DGE-1656518). N.E.R. acknowledges support from Intel SRC funding. Part of this work was performed at the Stanford Nano Shared Facilities (SNSF), supported by the National Science Foundation (Grant ECCS-1542152).

References:

(1) Gangnaik, A. S.; Georgiev, Y. M.; Holmes, J. D. New Generation Electron Beam Resists: A Review. *Chem. Mater.* **2017**, *29*, 1898–1917.

(2) Luo, C.; Xu, C.; Lv, L.; Li, H.; Huang, X.; Liu, W. Review of Recent Advances in Inorganic Photoresists. *RSC Adv.* **2020**, *10*, 8385–8395.

(3) Krysak, M.; Trikeriotis, M.; Schwartz, E.; Lafferty, N.; Xie, P.; Smith, B.; Zimmerman, P.; Montgomery, W.; Giannelis, E.; Ober, C. K. Development of an Inorganic Nanoparticle Photoresist for EUV, e-Beam, and 193nm Lithography. *Adv. Resist Mater. Process. Technol. XXVIII* **2011**, *7972*, 79721C.

(4) Trikeriotis, M.; Krysak, M.; Chung, Y. S.; Ouyang, C.; Cardineau, B.; Brainard, R.; Ober, C.

K.; Giannelis, E. P.; Cho, K. A New Inorganic EUV Resist with High-Etch Resistance. *Extrem. Ultrav. Lithogr. III* **2012**, *8322*, 83220U.

(5) Thakur, N.; Tseng, L.-T.; Vockenhuber, M.; Ekinci, Y.; Castellanos, S. Stability Studies on a Sensitive EUV Photoresist Based on Zinc Metal Oxoclusters. *J. Micro/Nanolithography, MEMS, MOEMS* **2019**, *18*, 1.

(6) Thrun, X.; Choi, K.-H.; Freitag, M.; Grenville, A.; Gutsch, M.; Hohle, C.; Stowers, J. K.; Bartha, J. W.; Toriumi, M.; Sato, Y.; Koshino, M.; Suenaga, K.; Itani, T.; Kumai, R.; Yamashita, Y.; Tsukiyama, K.; Itani, T.; Thakur, N.; Tseng, L.-T.; Vockenhuber, M.; Ekinci, Y.; Castellanos, S.; Luo, C.; Xu, C.; Lv, L.; Li, H.; Huang, X.; Liu, W.; Toriumi, M.; Sato, Y.; Koshino, M.; Suenaga, K.; Itani, T. Metal Resist for Extreme Ultraviolet Lithography Characterized by Scanning Transmission Electron Microscopy. *Appl. Phys. Express* **2016**, *9*, 97790G.

(7) Toriumi, M.; Sato, Y.; Koshino, M.; Suenaga, K.; Itani, T. Metal Resist for Extreme Ultraviolet Lithography Characterized by Scanning Transmission Electron Microscopy. *Appl. Phys. Express* **2016**, *9*.

(8) Saifullah, M. S. M.; Khan, M. Z. R.; Hasko, D. G.; Leong, E. S. P.; Neo, X. L.; Goh, E. T. L.; Anderson, D.; Jones, G. A. C.; Welland, M. E. Spin-Coatable HfO2 Resist for Optical and Electron Beam Lithographies. *J. Vac. Sci. Technol. B, Nanotechnol. Microelectron. Mater. Process. Meas. Phenom.* **2010**, *28*, 90–95.

(9) Stowers, J. K.; Telecky, A.; Kocsis, M.; Clark, B. L.; Keszler, D. A.; Grenville, A.; Anderson, C. N.; Naulleau, P. P. Directly Patterned Inorganic Hardmask for EUV Lithography. *Extrem.*

Ultrav. Lithogr. II **2011**, *7969*, 796915.

(10) Oleksak, R. P.; Ruther, R. E.; Luo, F.; Fairley, K. C.; Decker, S. R.; Stickle, W. F.; Johnson, D. W.; Garfunkel, E. L.; Herman, G. S.; Keszler, D. A. Chemical and Structural Investigation of High-Resolution Patterning with HafSOx. *ACS Appl. Mater. Interfaces* **2014**, *6*, 2917–2921.

(11) Toriumi, M.; Sato, Y.; Kumai, R.; Yamashita, Y.; Tsukiyama, K.; Itani, T. Characterization of "metal Resist" for EUV Lithography. *Adv. Patterning Mater. Process. XXXIII* **2016**, *9779*, 97790G.

(12) Sakai, K.; Xu, H.; Kosma, V.; Giannelis, E. P.; Ober, C. K. Progress in Metal Organic Cluster EUV Photoresists. *J. Vac. Sci. Technol. B* **2018**, *36*, 06J504.

(13) Pham, N. P.; Sarro, P. M.; Burghartz, J. N. <title>IC-Compatible Process for Pattern Transfer in Deep Wells for Integration of RF Components</Title>. *Micromach. Microfabr. Process Technol. VI* **2000**, *4174*, 390–397.

(14) Zhou, H.; Bent, S. F. Molecular Layer Deposition of Functional Thin Films for Advanced Lithographic Patterning. *ACS Appl. Mater. Interfaces* **2011**, *3*, 505–511.

(15) Zhou, H.; Blackwell, J. M.; Lee, H. B. R.; Bent, S. F. Highly Sensitive, Patternable Organic Films at the Nanoscale Made by Bottom-up Assembly. *ACS Appl. Mater. Interfaces* **2013**, *5*, 3691–3696.

(16) Nault, M. Single Layer Chemical Vapor Deposition Photoresist for 193 Nm Deep Ultraviolet Photolithography. *J. Vac. Sci. Technol. B Microelectron. Nanom. Struct.* **1998**, *16*, 3730.

(17) Wu, M. G.; Hsu, H. L.; Hsiao, K. W.; Hsieh, C. C.; Chen, H. Y. Vapor-Deposited Parylene Photoresist: A Multipotent Approach toward Chemically and Topographically Defined Biointerfaces. *Langmuir* **2012**, *28*, 14313–14322.

(18) Zhou, H.; Bent, S. F. Molecular Layer Deposition of Functional Thin Films for Advanced Lithographic Patterning. *ACS Appl. Mater. Interfaces* **2011**, *3*, 505–511.

(19) Sundberg, P.; Karppinen, M. Organic and Inorganic-Organic Thin Film Structures by Molecular Layer Deposition: A Review. *Beilstein J. Nanotechnol.* **2014**, *5*, 1104–1136.

(20) Mackus, A. J. M.; Schneider, J. R.; Macisaac, C.; Baker, J. G.; Bent, S. F. Synthesis of Doped, Ternary, and Quaternary Materials by Atomic Layer Deposition: A Review. *Chem. Mater.* **2019**, *31*, 1142–1183.

(21) Closser, K. D.; Ogletree, D. F.; Naulleau, P.; Prendergast, D. The Importance of Inner-Shell Electronic Structure for Enhancing the EUV Absorption of Photoresist Materials. *J. Chem. Phys.* **2017**, *146*.

(22) Pollentier, I.; Vesters, Y.; Jiang, J.; Vanelderen, P.; De Simone, D. Unraveling the Role of Secondary Electrons upon Their Interaction with Photoresist during EUV Exposure. *Proc. SPIE* **2017**, *10450*, 17.

(23) Bergsman, D. S.; Closser, R. G.; Tassone, C. J.; Clemens, B. M.; Nordlund, D.; Bent, S. F. Effect of Backbone Chemistry on the Structure of Polyurea Films Deposited by Molecular Layer Deposition. *Chem. Mater.* **2017**, *29*, 1192–1203.

(24) Closser, R. G.; Lillethorup, M.; Bergsman, D. S.; Bent, S. F. Growth of a Surface-Tethered,

All-Carbon Backboned Fluoropolymer by Photoactivated Molecular Layer Deposition. *ACS Appl. Mater. Interfaces* **2019**, *11*, 21988–21997.

(25) Richey, N. E.; Borhan, S.; Bent, S. F. Multi-Metal Coordination Polymers Grown through Hybrid Molecular Layer Deposition. *Dalt. Trans.* **2021**, *50*, 4577–4582.

(26) Lee, B. H.; Anderson, V. R.; George, S. M. Growth and Properties of Hafnicone and HfO2/Hafnicone Nanolaminate and Alloy Films Using Molecular Layer Deposition Techniques. *ACS Appl. Mater. Interfaces* **2014**, *6*, 16880–16887.

(27) Patel, D. I.; Tani, J. O.; Bahr, S.; Dietrich, P.; Meyer, M.; Thißen, A.; Matthew, R.; Patel, D. I.; Tani, J. O.; Bahr, S.; Dietrich, P.; Meyer, M.; Thißen, A.; Linford, M. R. Ethylene Glycol, by near-Ambient Pressure XPS. *Surf. Interface Anal.* **2019**, *26*, 024007–1.

(28) Barreca, D.; Milanov, A.; Fischer, R. A.; Devi, A.; Tondello, E. Hafnium Oxide Thin Film Grown by ALD: An XPS Study. *Surf. Sci. Spectra* **2007**, *14*, 34–40.

(29) Patel, D. I.; Tani, J. O.; Bahr, S.; Dietrich, P.; Meyer, M.; Thißen, A.; Matthew, R.; Patel, D. I.; Tani, J. O.; Bahr, S.; Dietrich, P.; Meyer, M.; Thißen, A.; Linford, M. R. Ethylene Glycol, by near-Ambient Pressure XPS. **2019**, *024007*.

(30) Rochat, N.; Dabertrand, K.; Cosnier, V.; Zoll, S.; Besson, P.; Weber, U. Infrared Spectroscopy of High k Thin Layer by Multiple Internal Reflection and Attenuated Total Reflection. *Phys. Status Solidi C Conf.* **2003**, *2965*, 2961–2965.

(31) Ho, M. T.; Wang, Y.; Brewer, R. T.; Wielunski, L. S.; Chabal, Y. J.; Moumen, N.; Boleslawski, M. In Situ Infrared Spectroscopy of Hafnium Oxide Growth on Hydrogen-Terminated

Silicon Surfaces by Atomic Layer Deposition. *Appl. Phys. Lett.* **2005**, *87*, 1–3.

(32) Asano, M. Sub-100 Nm Lithography Using KrF Exposure with Multiple Development Method. *1999 Int. Microprocess. Nanotechnol. Conf.* **1999**, No. December 1999, 154–155.

(33) Luo, X.; Li, Y.; Yang, H.; Liang, Y.; He, K.; Sun, W.; Lin, H. H.; Yao, S.; Lu, X.; Wan, L.; Feng, Z. Investigation of HfO2 Thin Films on Si by X-Ray Photoelectron Spectroscopy, Rutherford Backscattering, Grazing Incidence X-Ray Diffraction and Variable Angle Spectroscopic Ellipsometry. *Crystals* **2018**, *8*, 1–16.

(34) Gonzalez-Elipe, A. R.; Espinos, J. P.; Fernandez, A.; Munuera, G. XPS Study of the Surface Carbonation/Hydroxylation State of Metal Oxides. *Appl. Surf. Sci.* **1990**, *45*, 103–108.

(35) Nathawat, R.; Kumar, A.; Acharya, N. K.; Vijay, Y. K. XPS and AFM Surface Study of PMMA Irradiated by Electron Beam. *Surf. Coatings Technol.* **2009**, *203*, 2600–2604.

(36) Klepper, K. B.; Nilsen, O.; Hansen, P. A.; Fjellvåg, H. Atomic Layer Deposition of Organic-Inorganic Hybrid Materials Based on Saturated Linear Carboxylic Acids. *Dalt. Trans.* **2011**, *40*, 4636–4646.

(37) Li, F.; Koopal, L.; Tan, W. Roles of Different Types of Oxalate Surface Complexes in Dissolution Process of Ferrihydrite Aggregates. *Sci. Rep.* **2018**, *8*, 1–13.

(38) Li, F.; Koopal, L.; Tan, W. Roles of Different Types of Oxalate Surface Complexes in Dissolution Process of Ferrihydrite Aggregates. *Sci. Rep.* **2018**, *8*, 1–13.

(39) Uhl, A.; Bendig, J.; Leistner, J.; Jagdhold, U. A.; Bauer, J. J. E-Beam and Deep-UV Exposure of PMMA-Based Resists: Identical or Different Chemical Behavior? *Adv. Resist Technol.*

Process. XV **1998**, *3333*, 1452.

(40) Sear, R. P. Nucleation: Theory and Applications to Protein Solutions and Colloidal Suspensions. *J. Phys. Condens. Matter* **2007**, *19*.

(41) Polte, J. Fundamental Growth Principles of Colloidal Metal Nanoparticles - a New Perspective. *CrystEngComm* **2015**, *17*, 6809–6830.

(42) Thanh, N. T. K.; Maclean, N.; Mahiddine, S. Mechanisms of Nucleation and Growth of Nanoparticles in Solution. *Chem. Rev.* **2014**, *114*, 7610–7630.

(43) Wan, Y.; Zhou, X. Formation Mechanism of Hafnium Oxide Nanoparticles by a Hydrothermal Route. *RSC Adv.* **2017**, *7*, 7763–7773.

(44) Rossi, L. M.; Fiorio, J. L.; Garcia, M. A. S.; Ferraz, C. P. The Role and Fate of Capping Ligands in Colloidally Prepared Metal Nanoparticle Catalysts. *Dalt. Trans.* **2018**, *47*, 5889–5915.

(45) Li, L.; Chakrabarty, S.; Spyrou, K.; Ober, C. K.; Giannelis, E. P. Studying the Mechanism of Hybrid Nanoparticle Photoresists: Effect of Particle Size on Photopatterning. *Chem. Mater.* **2015**, *27*, 5027–5031.

(46) Wang, Y.; Firlar, E.; Dai, X.; Libera, M. Poly(Ethylene Glycol) as a Biointeractive Electron-Beam Resist. *J. Polym. Sci. Part B Polym. Phys.* **2013**, *51*, 1543–1554.

(47) Closser, K. D.; Ogletree, D. F.; Naulleau, P.; Prendergast, D. The Importance of Inner-Shell Electronic Structure for Enhancing the EUV Absorption of Photoresist Materials. *J. Chem. Phys.* **2017**, *146*.

(48) Park, H. H.; Zhang, X.; Lee, S. W.; Kim, K. D.; Choi, D. G.; Choi, J. H.; Lee, J.; Lee, E. S.; Park, H. H.; Hill, R. H.; Jeong, J. H. Facile Nanopatterning of Zirconium Dioxide Films via Direct Ultraviolet-Assisted Nanoimprint Lithography. *J. Mater. Chem.* **2011**, *21*, 657–662.

(49) Stehlin, F.; Wieder, F.; Spangenberg, A.; Le Meins, J. M.; Soppera, O. Room-Temperature Preparation of Metal-Oxide Nanostructures by DUV Lithography from Metal-Oxo Clusters. *J. Mater. Chem. C* **2014**, *2*, 277–285.

(50) Park, H. H.; Law, W. L.; Zhang, X.; Hwang, S. Y.; Jung, S. H.; Shin, H. B.; Kang, H. K.; Park, H. H.; Hill, R. H.; Ko, C. K. Facile Size-Tunable Fabrication of Functional Tin Dioxide Nanostructures by Multiple Size Reduction Lithography. *ACS Appl. Mater. Interfaces* **2012**, *4*, 2507–2514.

TOC Figure:

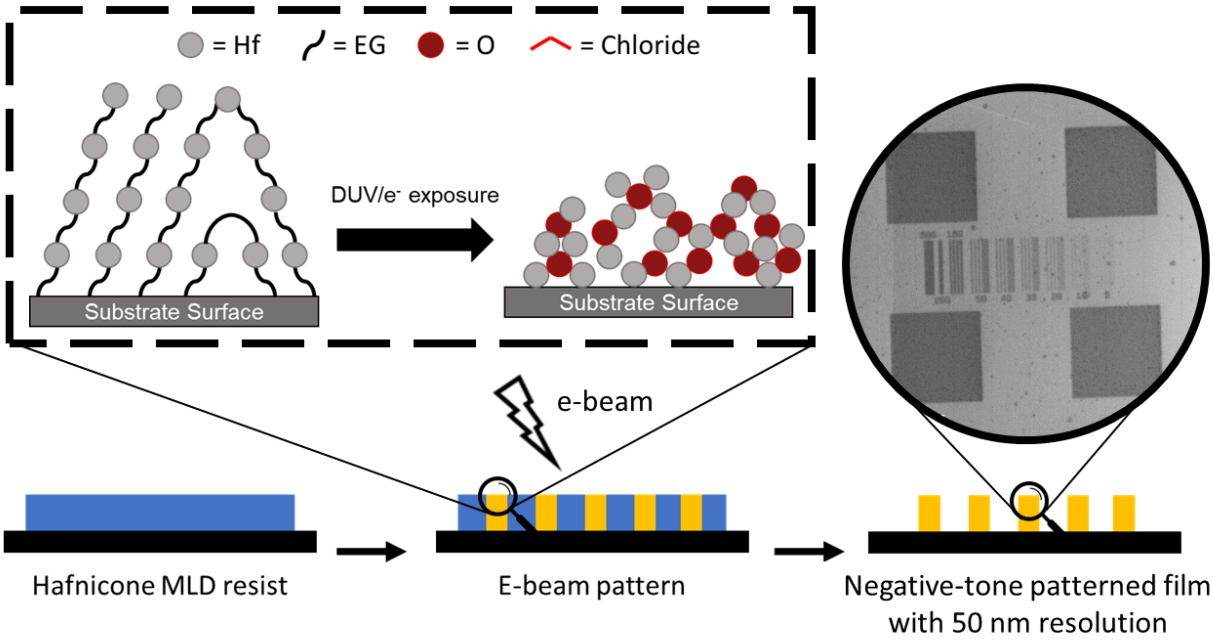
= Hf
= EG
= O
= Chloride
DUV/e- exposure
Substrate Surface
Substrate Surface
e-beam
Hafnicone MLD resist
E-beam pattern
Negative-tone patterned film
with 50 nm resolution